Chemical Science

ROYAL SOCIETY OF CHEMISTRY

EDGE ARTICLE

View Article Online
View Journal | View Issue

Open Access Article. Published on 03 2022. Downloaded on 01.02.2026 18:25:54.
This article is licensed under a Creative Commons Attribution-NonCommercial 3.0 Unported Licence.

Check for updates

Cite this: *Chem. Sci.*, 2022, **13**, 13764

All publication charges for this article have been paid for by the Royal Society of Chemistry

Room temperature chemoselective hydrogenation of C=C, C=O and C=N bonds by using a well-defined mixed donor Mn(I) pincer catalyst†

Anand B. Shabade,[ab] Dipesh M. Sharma,[ab] Priyam Bajpai,[bc] Rajesh G. Gonnade,[bd] Kumar Vanka[bc] and Benudhar Punji *[ab]

Received 21st September 2022
Accepted 2nd November 2022

DOI: 10.1039/d2sc05274a

rsc.li/chemical-science

Chemoselective hydrogenation of C=C, C=O and C=N bonds in α,β-unsaturated ketones, aldehydes and imines is accomplished at room temperature (27 °C) using a well-defined Mn(I) catalyst and 5.0 bar H_2. Amongst the three mixed-donor Mn(I) complexes developed, κ^3-($^{R2}PN^3N^{Pyz}$)Mn(CO)$_2$Br (R = Ph, ^{i}Pr, ^{t}Bu); the ^{t}Bu-substituted complex ($^{tBu2}PN^3N^{Pyz}$)Mn(CO)$_2$Br shows exceptional chemoselective catalytic reduction of unsaturated bonds. This hydrogenation protocol tolerates a range of highly susceptible functionalities, such as halides (–F, –Cl, –Br, and –I), alkoxy and hydroxy, including hydrogen-sensitive moieties like acetyl, nitrile, nitro, epoxide, and unconjugated alkenyl and alkynyl groups. Additionally, the disclosed method applies to indole, pyrrole, furan, thiophene, and pyridine-containing unsaturated ketones leading to the corresponding saturated ketones. The C=C bond is chemoselectively hydrogenated in α,β-unsaturated ketones, while the aldehyde's C=O bond and imine's C=N bond are preferentially reduced over the C=C bond. A detailed mechanistic study highlighted the non-innocent behavior of the ligand in the ($^{tBu2}PN^3N^{Pyz}$)Mn(I) complex and indicated a metal–ligand cooperative catalytic pathway. The molecular hydrogen (H_2) acts as a hydride source, whereas MeOH provides a proton for hydrogenation. DFT energy calculations supported the facile progress of most catalytic steps, involving a crucial turnover-limiting H_2 activation.

Introduction

Chemoselective hydrogenation of unsaturated organic compounds is extremely important in academia and industry, as it plays a crucial role in the preparation of pharmaceutical intermediates, fragrances, fine chemicals and various bulk products. Particularly, the catalytic reductions using molecular hydrogen under ambient conditions represent one of the economical, atom-efficient and environmentally benign transformations.[1] In this context, numerous heterogeneous catalysts are developed and demonstrated for the hydrogenation of various functional groups, which often require high reaction temperatures and/or pressures and result in poor selectivity.[2] Over time, many well-defined, active and highly efficient homogeneous catalysts,[3] derived from precious and non-precious transition metals, have been established for hydrogenation.[4] In general, noble metal catalysis has dominated the field and accomplished very high catalytic turnovers and desired selectivity. However, the limited availability of noble metals in the earth's crust, and their expensiveness and underlying toxicity could limit their wide applications in hydrogenation in the future.

One of the fundamental research objectives in modern science is environmental benignity and sustainable development. Accordingly, the hydrogenations by catalysts based on low-toxic, earth-abundant and inexpensive non-precious metals have been given significant consideration.[5] Particularly, the hydrogenations employing iron,[6] cobalt[7] and nickel[6c] are substantially explored and disclosed as active and highly efficient for reducing carbonyls, imines and nitriles.[8] Being a less toxic, cheap and the third most abundant transition metal, manganese is elegantly demonstrated as a catalyst for the hydrogenation of aldehydes/ketones by Beller,[9] Kempe,[10] Sortais,[11] Kirchner[12] and others (Scheme 1a).[13,14] Similarly, the hydrogenation of imines (or C=N bond) using bidentate or pincer-ligated manganese catalysts was established.[15] Meanwhile, the independent development of chiral pincer-manganese catalysts by Clarke,[16] Beller,[17] Han/Ding[18] and others[19] led to the asymmetric hydrogenation of ketones. In

[a]*Organic Chemistry Division, CSIR-National Chemical Laboratory (CSIR-NCL), Dr Homi Bhabha Road, Pune 411008, India. E-mail: b.punji@ncl.res.in*

[b]*Academy of Scientific and Innovative Research (AcSIR), Ghaziabad 201002, India*

[c]*Physical and Material Chemistry Division, CSIR-NCL, Dr Homi Bhabha Road, Pune, India*

[d]*Centre for Material Characterization, CSIR-NCL, Dr Homi Bhabha Road, Pune, India*

† Electronic supplementary information (ESI) available: Full experimental procedures and characterization data, including ^{1}H and ^{13}C NMR of all compounds, CIF and DFT (.xyz) file]. CCDC 2194541 (for comp. **Mn-2**). For ESI and crystallographic data in CIF or other electronic format see DOI: https://doi.org/10.1039/d2sc05274a

© 2022 The Author(s). Published by the Royal Society of Chemistry

Open Access Article. Published on 03 2022. Downloaded on 01.02.2026 18:25:54.
This article is licensed under a Creative Commons Attribution-NonCommercial 3.0 Unported Licence.

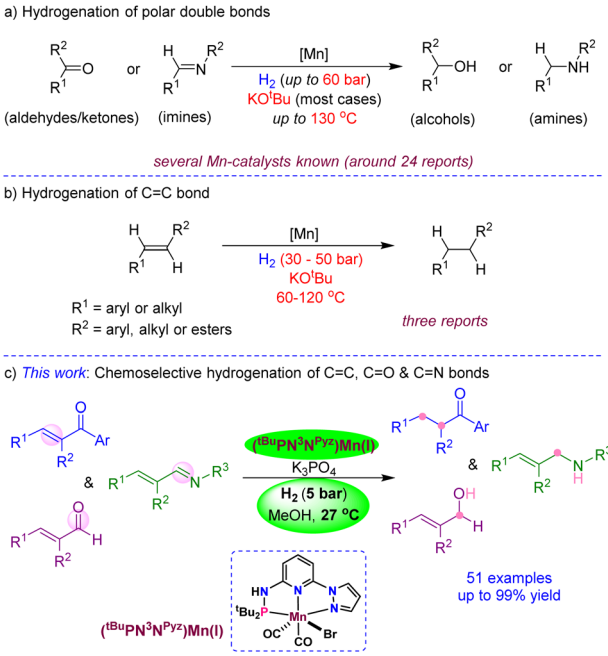

Scheme 1 Manganese-catalyzed hydrogenation of unsaturated bonds: (a) carbonyls and imines, (b) C=C bond, and (c) chemoselective hydrogenation of C=C, C=O, and C=N bonds.

a significant advancement, Liu has shown the asymmetric hydrogenation of the C=N bond in heteroaromatics using a chiral Mn-catalyst.[20] Despite all developments on the Mn-catalyzed hydrogenations of multiple polar bonds, the chemoselective hydrogenation of C=C bonds is highly challenging and extremely rare due to the associated high bond enthalpies. The group of Kirchner and Khusnutdinova independently used bidentate PP- and PN-ligated Mn(I) catalysts for the hydrogenation of alkenes using 50 bar and 30 bar H_2 pressures, respectively, at elevated temperatures (Scheme 1b).[21] Similarly, Topf has demonstrated C=C hydrogenation in α,β-unsaturated carboxylic derivatives using 30–50 bar H_2 at 100–120 °C; however, this protocol failed to provide chemoselective hydrogenation in α,β-unsaturated ketones.[13c] Though manganese-based catalysts promoted the hydrogenations of many C=O and C=N bonds and certain C=C bonds,[11b,13c,21] most of the reactions proceed at a high H_2 pressure and at elevated temperatures, which is a significant drawback for practical applications. Additionally, most Mn-catalyzed hydrogenations require a large amount of a strong base (KO^tBu) as an additive. As yet, a chemoselective hydrogenation protocol for reducing one unsaturated functional moiety in the presence of the other using a beneficial Mn-catalyst at ambient H_2 pressure and temperature is unknown.[22]

To achieve more sustainability, efficiency and selectivity in Mn-catalysis, in this work, we developed the mixed-donor (PN^3N)Mn(I) complexes and disclosed the chemoselective hydrogenation of C=C, C=O and C=N bonds using 5 bar H_2 and a mild base K_3PO_4 at room temperature (Scheme 1c). The notable features of the present protocol are (i) use of the 3rd most abundant transition metal as a catalyst, (ii) excellent chemoselectivity in the reduction of C=C, C=O and C=N bonds, (iii) hydrogenation using 5 bar H_2 and at room temperature (27 °C), (iv) use of a mild base and atom-efficient H_2 source, and (v) broad substrates scope with excellent tolerance of hydrogen-sensitive functionalities.

Results and discussion

Synthesis of Mn(I) complexes

Based on our expertise in developing pincer-ligated complexes, we became interested in synthesizing mixed-donor PN^3N ligands and pincer manganese complexes. We envisioned that a mixed-donor ligand with different electronic features of the donating center could suitably administer the electronic requirement at the metal center and can stabilize the active catalytic species. Moreover, the presence of NH on the side-arm could facilitate the non-innocent behavior of the ligand *via* an aromatization/dearomatization approach leading to the heterolytic activation of molecules. With this in mind, the isopropyl-tagged PN^3N ligand **L2** was synthesized in a few steps starting from 2,6-dibromopyridine, following a protocol similar to that for the synthesis of phenyl or *tert*-butyl PN^3N ligands **L1** and **L3**.[23] Treatment of pincer ligands **L1–L3** with $Mn(CO)_5Br$ in THF at room temperature afforded dicarbonyl Mn(I) complexes, ($^{R2}PN^3N^{Pyz}$)$Mn(CO)_2Br$; **Mn-1** (R = Ph), **Mn-2** (R = ^{i}Pr) and **Mn-3** (R = ^{t}Bu), respectively, in good yields (Scheme 2). These complexes were extensively characterized by multinuclear NMR spectroscopy, FT-IR, ESI-MS and elemental analysis. The $^{31}P\{^1H\}$-NMR spectra of complexes **Mn-1**, **Mn-2** and **Mn-3** show peaks at 134.5, 136.9; 158.4, 159.8 and 175.3, 178.5 ppm, respectively. Two peaks for each complex at very similar chemical shift values indicate the formation of two geometrical isomers for each complex. Interestingly, all complexes displayed three IR peaks for carbonyls ranging between 1857 and 2053 cm^{-1}. Similarly, a closer look at the $^{13}C\{^1H\}$-NMR spectra of complexes indicates the three carbonyl signals. Moreover, the ^1H and $^{13}C\{^1H\}$-NMR spectra of all complexes display two sets of peaks. All these observations support the formation of two geometrical isomeric species in each complex **Mn-1**, **Mn-2** and **Mn-3**. Considering the presence of three signals for carbonyls in each complex, we assume that one isomer of the Mn-complex would have two carbonyls that are *trans* to –Br and $-N_{py}$ ligands accounting for two peaks (as indicated in the X-ray

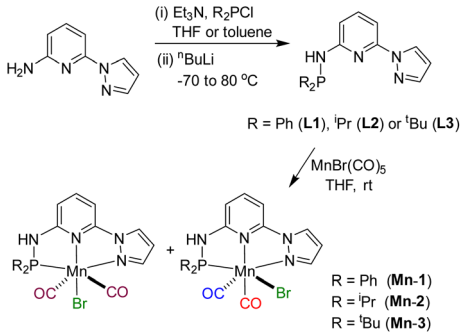

Scheme 2 Synthesis of ($^{R2}PN^3N^{Pyz}$) manganese pincer complexes.

Open Access Article. Published on 03 2022. Downloaded on 01.02.2026 18:25:54.
This article is licensed under a Creative Commons Attribution-NonCommercial 3.0 Unported Licence.

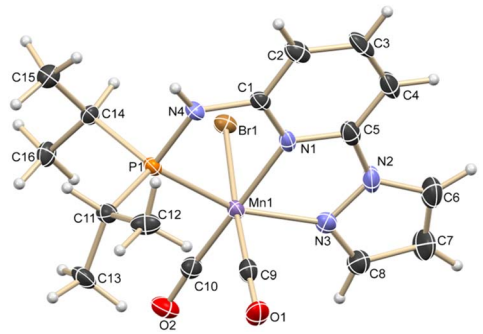

Fig. 1 ORTEP of compound **Mn-2** showing the atom-numbering scheme. Displacement ellipsoids are drawn at the 50% probability level. Selected bond length (Å): Br1–Mn1, 2.5916(7); Mn1–C9, 1.773(4); Mn1–C10, 1.797(4); Mn1–N3, 2.011(3); Mn1–N1, 2.012(3); Mn1–P1, 2.2462(12). Selected bond angles (°): N3–Mn1–P1, 160.49(11); C10–Mn1–N1, 175.88(16); C9–Mn1–Br1, 175.54(14); C9–Mn1–C10, 87.40(19); C9–Mn1–N1, 96.23(16); N1–Mn1–Br1, 84.57(9).

structure), whereas the other isomer would have two carbonyls *trans* to each other and display a single carbonyl peak (Scheme 2). Even though the assumed isomers are highly convincing, the probability of the mixture of a neutral (with –Br coordination) and a cationic (with Br as an anion) manganese species cannot be completely ruled out.[11a,13b,16,17a] All the complexes are further characterized by ESI-MS that show two prominent isotopic masses for ^{79}Br and ^{81}Br containing complexes. The molecular structure of **Mn-2** was confirmed by a single crystal X-ray study (Fig. 1). As expected, the coordination geometry around the manganese is distorted octahedral with –Br and one –CO unit *trans* to each other, making the C9–Mn1–Br angle almost linear (175.54(15)°). The Mn1–C10 bond length (1.797(4) Å) is slightly longer than the Mn1–C9 bond length (1.773(4) Å), which might be due to the greater *trans* influence of $-N_{py}$ than the –Br. Although each synthesized manganese complex contains two isomeric species, the generated active catalyst in the presence of a base is expected to be a single isomer (proved and discussed *vide infra*).

Optimization for catalytic hydrogenation

After synthesizing the sterically and electronically distinct mixed-donor (PN^3N) manganese complexes, we have investigated their catalytic behavior for the chemoselective hydrogenation of α,β-unsaturated ketones using molecular hydrogen. We first screened the activity of (PN^3N)Mn(I) complexes **Mn-1**, **Mn-2**, and **Mn-3** for C=C bond hydrogenation in (*E*)-3-phenyl-1-(phenyl)prop-2-en-1-one (**4a**) using a catalytic amount of KO^{t}Bu and 30 bar hydrogen pressure in methanol at 50 °C (see, Tables 1 and S1 in the ESI†). The use of **Mn-1** as a catalyst led to 75% conversion of **4a**, wherein chemoselective C=C hydrogenated product **4** was obtained in 65% yield, and completely

Table 1 Optimization of reaction conditions[a]

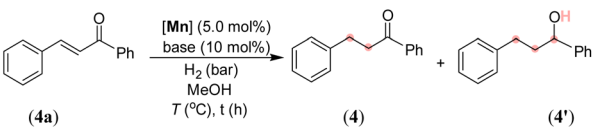

(**4a**) (**4**) (**4'**)

Entry	[Mn]	Base	T (°C)/t (h)	Conv.[b] (%)	**4** [b] (%)	**4'** [b] (%)
1	**Mn-1**	KO^{t}Bu	50/20	75	65	10
2[c]	**Mn-2**	KO^{t}Bu	50/20	100	—	80
3	**Mn-3**	KO^{t}Bu	50/20	100	63 (60)	37
4	**Mn-3**	KO^{t}Bu	27/20	100	81 (79)	19
5	**Mn-3**	KO^{t}Bu	27/20	100	91 (88)	9
6	**Mn-3**	NaO^{t}Bu	27/20	40	39	Trace
7	**Mn-3**	LiO^{t}Bu	27/20	74	73	Trace
8	**Mn-3**	K_2CO_3	27/20	100	74	26
9	**Mn-3**	KOAc	27/20	20	19	Trace
10	**Mn-3**	K_3PO_4	27/20	100	88	12
11	**Mn-3**	**K_3PO_4**	**27/1**	**100**	**98 (96)**	**2**
12	$Mn(CO)_5Br$/**L3**	K_3PO_4	27/1	39	39	—
13	$MnBr_2$/**L3**	K_3PO_4	27/1	—	—	—
14	$MnCl_2$/**L3**	K_3PO_4	27/1	—	—	—

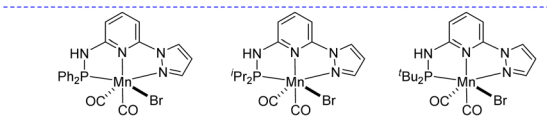

(**Mn-1**) (**Mn-2**) (**Mn-3**)

[a] Reaction conditions: **4a** (0.042 g, 0.20 mmol), base (0.02 mmol), [Mn] catalyst (0.01 mmol, 5 mol%), solvent (1.0 mL). Entries 1–4: 30 bar H_2; entries 5–10: 10 bar H_2; entries 11–14: 5 bar H_2. [b] GC conversion, isolated yields are given in parentheses. [c] 20% allylic alcohol was observed. All the catalysts **Mn-1**, **Mn-2** and **Mn-3** contain a mixture of two geometrical isomers.

© 2022 The Author(s). Published by the Royal Society of Chemistry

Open Access Article. Published on 03 2022. Downloaded on 01.02.2026 18:25:54.
This article is licensed under a Creative Commons Attribution-NonCommercial 3.0 Unported Licence.

hydrogenated compound **4′** in 10% yield (entry 1). The electronically rich complex **Mn-2** gave complete conversion of **4a**; however, the product **4′** was obtained in 80% yield, and the remaining was allylic alcohol with only C=O hydrogenation (entry 2). Interestingly, the bulky ^{t}Bu-substituted complex **Mn-3** gave a complete conversion of **4a** with more chemoselectivity for **4** (entry 3). The formation of allylic alcohol in the presence of catalyst **Mn-2** suggests the probability of a sequential C=O hydrogenation-allylic alcohol isomerization leading to the uncontrolled hydrogenated compound **4′**. The low steric effect in complex **Mn-2** compared to **Mn-3** might play a crucial role in chemoselective hydrogenation (1,2-hydrogenation of C=O *versus* 1,4-hydrogenation of C=C). Notably, the reaction at lower hydrogen pressure and room temperature (27 °C) significantly improved chemoselective C=C bond hydrogenation without altering the overall conversion (entries 4 and 5). The use of other bases, such as NaO^{t}Bu, LiO^{t}Bu, and KOAc, led to low conversion, whereas the presence of mild bases K_2CO_3 or K_3PO_4 provided complete conversion with good chemoselectivity for **4** using 10 bar H_2 and at room temperature (entries 6–10). The activity of a manganese catalyst using a catalytic amount of mild base K_3PO_4 is notable, as most of the Mn catalysis generally employs a strong base like KO^{t}Bu. The chemoselective hydrogenation of **4a** also proceeded smoothly using 5 bar hydrogen pressure at room temperature (27 °C) and provided **4** in 96% isolated yield just in an hour (entry 11). Notably, the manganese catalysts **Mn-1** and **Mn-2** were less effective for hydrogenation under the optimized conditions (5 bar H_2/27 °C/1 h), and provided <19% of product **4** (see the ESI†). Therefore, all chemoselective hydrogenations were conducted employing the **Mn-3** catalyst and 5 bar H_2 pressure at room temperature with the best-optimized reaction time. An *in situ* generated $Mn(CO)_5Br$/**L3** catalyst system is less effective, affording the hydrogenated product in 39% yield, highlighting the importance of a well-defined manganese catalyst (entry 12). However, a Mn(II) precursor with the **L3** ligand ($MnCl_2$/**L3** or $MnBr_2$/**L3**) did not provide hydrogenation (entries 13 and 14). Similarly, the $Mn(CO)_5Br$ precursor and bidentate N-donor or P-donor ligand systems were ineffective. Hydrogenation did not proceed in the absence of a catalyst, a base or H_2, which suggests the importance of these components for the reaction.

Substrate scope of hydrogenation

After successfully optimizing the reaction parameters for chemoselective C=C bond hydrogenation in chalcone, we have explored the reaction scope using catalyst **Mn-3**, catalytic K_3PO_4 and 5 bar H_2 at room temperature (Scheme 3). Depending upon the substrates, the hydrogenations were performed for different time intervals, and the best yields were reported. First, we checked the hydrogenation of α,β-unsaturated ketones with different substitutions on the benzoyl ring. Thus, the chalcones containing electron-donating alkyl and alkoxy substitutions at the *para* position of benzoyl reacted smoothly to give a good to an excellent yield of saturated ketones **5–7**. The halogen substitutions, –Cl, –Br, –I, and –CF_3, were well tolerated at the *para* position of the benzoyl ring affording the desired saturated ketones (**8–11**) in good yields. The tolerance of such functionalities is noteworthy as they can be employed for late-stage diversification. In addition to the *para*-substituted chalcones, the electron-rich and electron-deficient *ortho*-substituted compounds smoothly participated in hydrogenation (**12** and **13**). Chalcone having a phenolic –OH at the *meta* position of benzoyl, reacted slowly and afforded the product **14** in 33% yield. Interestingly, unsaturated ketones with sensitive and reducible functionalities, such as terminal alkene, alkyne, and epoxide, reacted chemoselectively to give compounds **15–17**. The unsaturated ketones with the naphthyl moiety also reacted with good yields (**18** and **19**). A higher-scale hydrogenation of compound **4a** (0.5 g, 2.4 mmol) provided the product **4** in 87% isolated yield (Scheme 3, in parenthesis), highlighting the potential practical application.

After this, we moved to check the effect and tolerability of different substitutions on the alkenyl–arenes towards chemoselective hydrogenation. Substrates with electron-rich substituents such as phenyl, methoxy and benzyloxy reacted efficiently, producing excellent yields of products **20–22**. The survival of benzyl protection of phenolic –OH is notable, as such substrates are prone to hydrogenolysis under hydrogenation conditions. Similarly, the –Cl and –CF_3 groups remained unaffected and delivered the saturated halo-ketones **23** and **24** in 80% and 96% yields, respectively. An amine functionality that could poison catalysis by binding to the metal is also sustained under optimized conditions (**25**). To our surprise, the highly desirous and hydrogenation-sensitive functionalities, –CN and –NO_2 groups, could be tolerated to afford the products **26** and **28** in around 88% yields. A range of α,β-unsaturated ketones derived from heteroarenes, such as furanyl, thiophenyl, indolyl, pyrrolyl and pyridinyl, were successfully hydrogenated to afford the saturated heteroaryl ketones (**30–35**). The chemoselective hydrogenation of these heteroaryl-containing compounds is remarkable, as the heteroaryl rings often interfere with the reaction due to their coordination ability to metal. The hydrogenation of ketones having unprotected NH indolyl and pyrrolyl opens up a new avenue as they can further be diversified. An unsaturated ketone containing a ferrocene backbone provided selective hydrogenation to **36** in 72% yield. Interestingly, hydrogenation of a ketone containing extended conjugation provided selectively semi-hydrogenated product **37** in 78% yield. Similarly, in the substrate where the carbonyl group is in conjugation with two alkenes, one C=C bond was selectively hydrogenated and provided a good yield of product **38**. This hydrogenation protocol is also suitable for α,β-unsaturated ketones having a trisubstituted alkene to provide saturated ketones, albeit in moderate yields (**39** and **40**). A β-alkyl-α,β-unsaturated ketone, (*E*)-1-phenyloct-2-en-1-one could be hydrogenated to give compound **41** in 75% yield. Interestingly, in all these cases, an excellent chemoselective C=C bond hydrogenation was observed in the presence of other H_2-sensitive functionalities. Such chemoselective hydrogenation employing a Mn-catalyst is extremely rare.[11b,12c,13c] Unfortunately, the α,β-unsaturated ketones with free –OH at the *ortho* position, and carboxylate, ester and amide derivatives failed to participate in the reaction under the optimized conditions. However, the substrate (*E*)-4-phenylbut-

Open Access Article. Published on 03 2022. Downloaded on 01.02.2026 18:25:54.
This article is licensed under a Creative Commons Attribution-NonCommercial 3.0 Unported Licence.

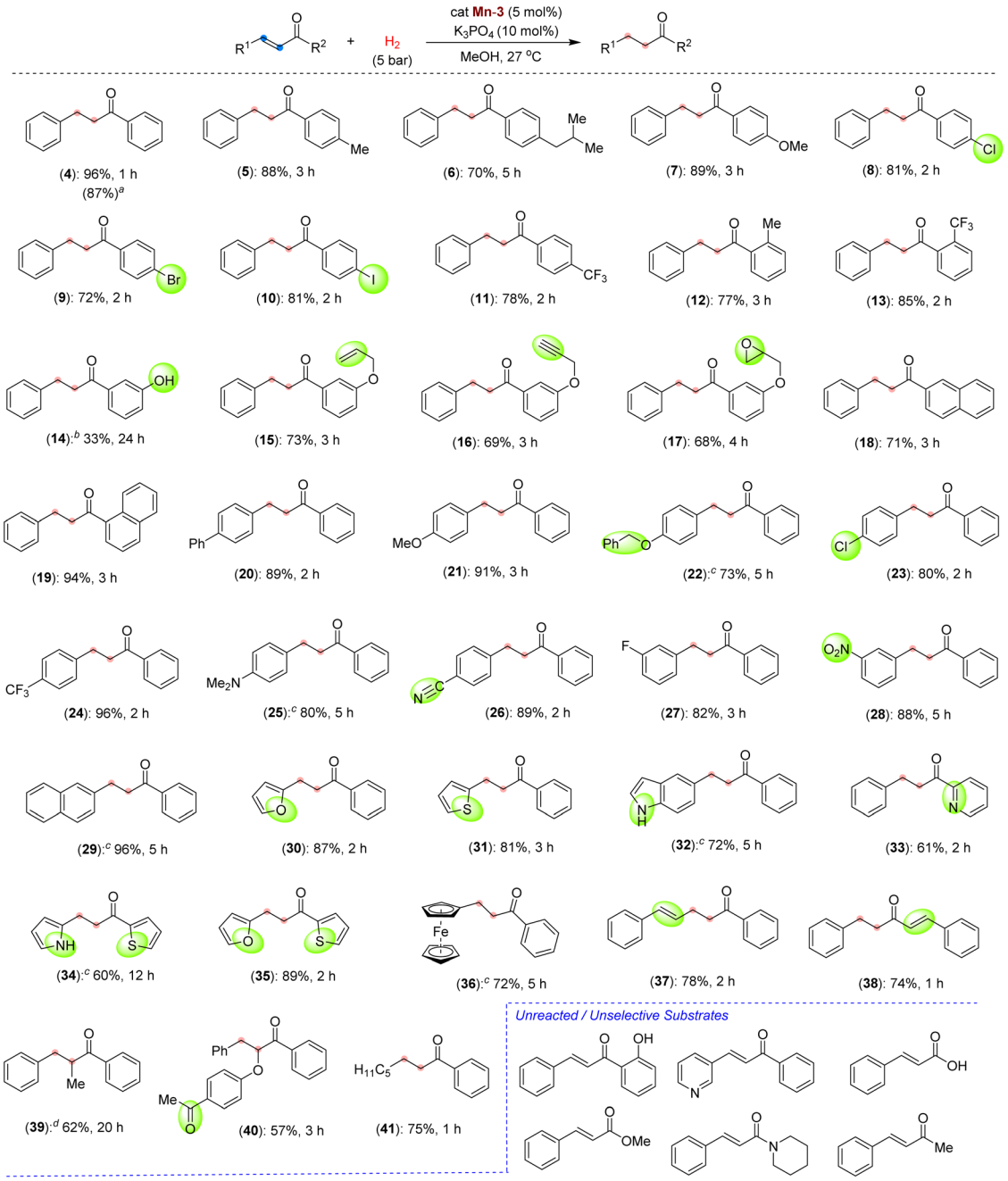

Scheme 3 Scope of Mn-catalyzed C=C bond hydrogenation of α,β-unsaturated ketones. Reaction conditions: substrate, α,β-unsaturated ketone (0.20 mmol), **Mn-3** (0.005 g, 0.01 mmol, 5 mol%), K_3PO_4 (0.0043 g, 0.02 mmol), MeOH (1.0 mL), H_2 (5 bar). Yields are of isolated compounds. [a]Reaction in 0.5 g scale. [b]Reaction at 50 °C. [c]Mixture of MeOH : DCM (4 : 1) used. [d]Reaction at 10 bar H_2 and 50 °C.

3-en-2-one gave a mixture of highly unselective hydrogenated products.

After exploring the scope and limitations of selective C=C bond hydrogenation in unsaturated ketones, we were eager to know the reactivity of the synthesized manganese complex on the hydrogenation of α,β-unsaturated aldehydes and imines (Scheme 4). Surprisingly, under the standard reaction conditions, selective C=O bond hydrogenation of cinnamaldehyde derivatives was observed, leading to the 3-phenylprop-2-en-1-ols (**42**–**44**) in excellent yields. Aliphatic and acyclic conjugated aldehydes also participated in the selective hydrogenation to unsaturated alcohols without harming the alkenyl groups, thus leading to the products **45** and **46** in 77% and 73% yields, respectively. The aromatic aldehydes containing benzyloxy, nitro, –OH, and pyrrolyl groups were also smoothly hydrogenated to the corresponding alcohols at room temperature (**48**–**52**). The tolerance of free –OH and –NH groups is highly impressive. Similarly, an α,β-unsaturated imine was chemoselectively hydrogenated to unsaturated amine (**53**) in good yield. Even a simple unconjugated *N*-aryl imine could be

© 2022 The Author(s). Published by the Royal Society of Chemistry

Open Access Article. Published on 03 2022. Downloaded on 01.02.2026 18:25:54.
This article is licensed under a Creative Commons Attribution-NonCommercial 3.0 Unported Licence.

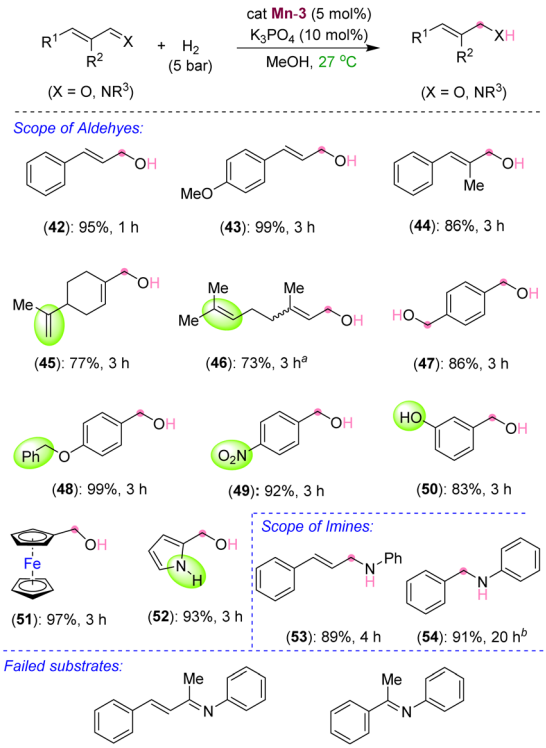

Scheme 4 Scope of Mn-catalyzed hydrogenation of aldehydes and imines. [a]Reaction conditions: substrate (0.20 mmol), **Mn-3** (0.005 g, 0.01 mmol, 5 mol%), K_3PO_4 (0.0043 g, 0.02 mmol), H_2 (5 bar), MeOH (1.0 mL). Yields are of isolated compounds. [a]Obtained as a mixture of *E* and *Z* isomers as the starting compound was also a mixture of both. [b]Reaction performed at 50 °C.

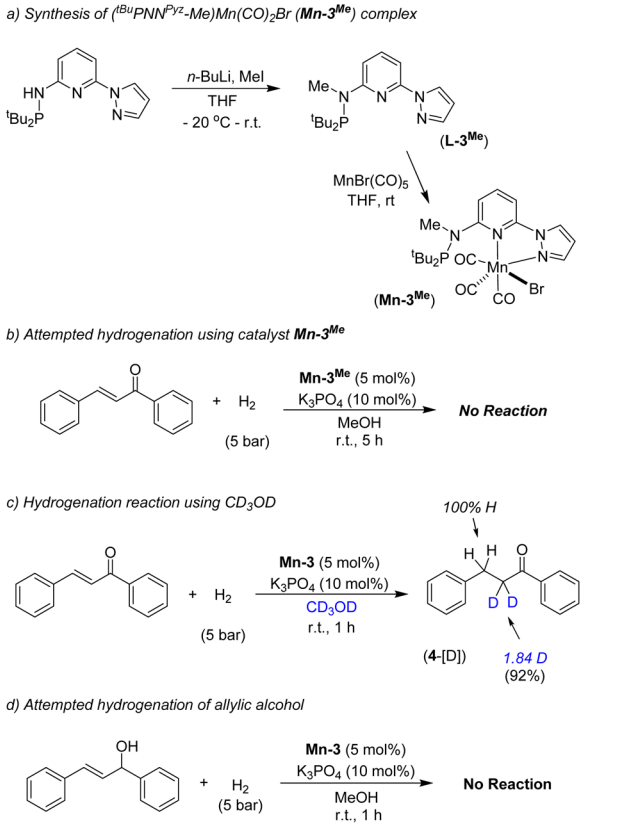

Scheme 5 Synthesis of **Mn-3**^{Me} and controlled mechanistic experiments.

hydrogenated to amine in high yield (**54**). However, the attempted hydrogenations of ketone-derived imine analogues, such as (2*E*,3*E*)-*N*,4-diphenylbut-3-en-2-imine and (*E*)-*N*,1-diphenylethan-1-imine, failed under the optimized conditions and the unreacted starting compounds were quantitatively recovered (Scheme 4). We assume that the steric hindrance around the keto-derived imine inhibited its approach towards the manganese center, leading to an unsuccessful reaction. The chemoselective hydrogenations of the C=C bond over the ketone carbonyl and that of the aldehyde's C=O and imine's C=N over the C=C by using the newly developed catalyst are notable. Particularly, mild reaction conditions and the use of the catalytic K_3PO_4 base are significant. This catalyst can further be applied to novel catalytic approaches considering its advantage over other similar catalysts. Though, an excellent chemoselectivity was observed in the hydrogenation of α,β-unsaturated ketones, a trace formation of both C=C and C=O reductions was unavoidable in some cases.

Mechanistic aspects

We have performed a few controlled experiments to understand the operating mode of the manganese catalyst. First, the *N*-methyl substituted ligand (**L3-Me**) and corresponding manganese complex, (^{tBu}PN(Me)N^{Pyz})Mn(CO)$_3$Br (**Mn-3**^{Me}) were synthesized and fully characterized by various analytical techniques (Scheme 5a). An attempted hydrogenation of **4a** employing complex **Mn-3**^{Me} as the catalyst under the standard hydrogenation conditions did not provide the hydrogenated product (Scheme 5b), and the starting compound (**4a**) was quantitatively recovered. This finding supports the crucial role of the N–H proton in the complex (^{tBu}PN^3(H)N^{Pyz})Mn(CO)$_2$Br (**Mn-3**) during hydrogenation. Furthermore, the treatment of **Mn-3** with stoichiometric KO^{t}Bu produced dearomatized active intermediate **A** (Fig. 2). The ^{31}P{^{1}H} NMR spectrum of **A** showed a single peak (against two isomeric peaks for **Mn-3**), and two CO signals were observed in IR as well as ^{13}C{^{1}H} NMR spectra of **A** (against three peaks for CO in **Mn-3**). Interestingly, the employment of species **A** as a catalyst in hydrogenation without the use of an additional base provided a quantitative yield of **4**. All these results suggest that the species **A** acts as an active catalyst and the catalytic reaction proceeds through the metal–ligand cooperation (dearomatization/aromatization) pathway.

A hydrogenation reaction was performed using CD_3OD as a solvent to thoroughly understand the hydrogenation process (Scheme 5c). The isolated hydrogenated product **4**-[D] shows 92% deuterium incorporation at the alpha-methylene position (see ^{1}H, ^{13}C and deuterium NMR spectra in the ESI†). Moreover, the hydrogenation reaction did not occur in the presence of aprotic solvent (THF, dioxane or CH_2Cl_2). These observations indicate the necessity of a protic solvent as a proton source and

Open Access Article. Published on 03 2022. Downloaded on 01.02.2026 18:25:54.
This article is licensed under a Creative Commons Attribution-NonCommercial 3.0 Unported Licence.

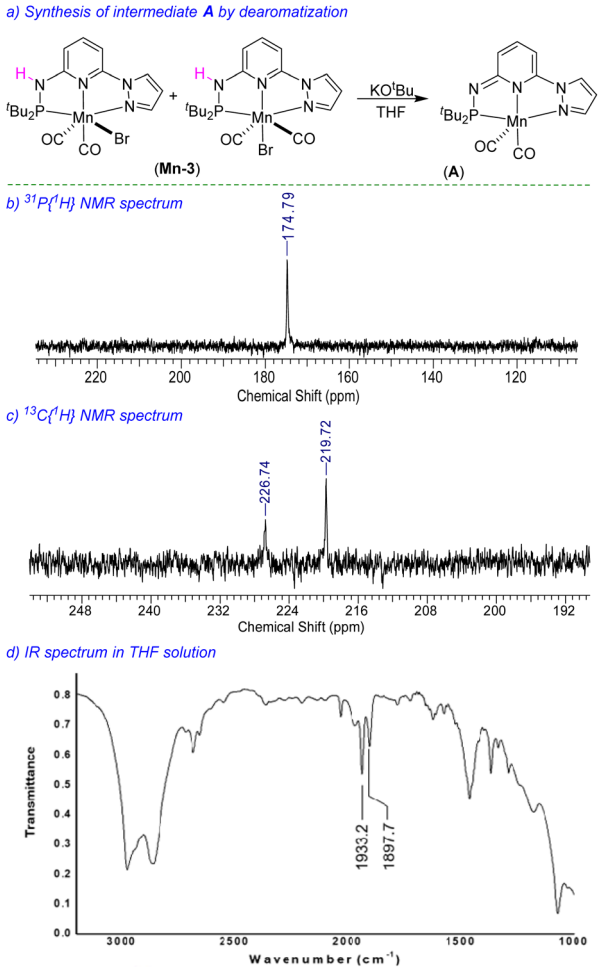

Fig. 2 Synthesis of active intermediate A and characterization spectra.

tentatively support a Mn-enolate intermediate. All these findings are consistent with the low energy barrier observed for the protonation step (discussed *vide infra*). An attempted hydrogenation of allylic alcohol under the standard reaction conditions failed to give a hydrogenated product (Scheme 5d). This finding highlights that the hydrogenation of (*E*)-chalcone (**4a**) does not proceed *via* 1,2-hydrogen addition, instead a 1,4-addition of hydrogen occurs. The observed chemoselectivity and controlled studies allowed us to propose the following: (i) the **Mn-3** catalyst prefers 1,2-hydrogen addition to C=O or C=N when steric hindrance on carbonyl's/imine's carbon is low (aldehyde's C=O and imine's C=N preferred over the C=C), whereas (ii) the **Mn-3** catalyst allowed 1,4-hydrogen addition when carbonyl's carbon is doubly substituted (*i.e.* in α,β-unsaturated ketones) due to more steric constraint. Mn–H might fail to approach the carbonyl's carbon in α,β-unsaturated ketones due to steric hindrance; instead it can access the β-carbon *via* 1,4-hydrogen addition. Notably, the **Mn-2** catalyst, which is less bulky than the **Mn-3** catalyst, allowed 1,2-hydrogen addition even in α,β-unsaturated ketone to form allylic alcohol. These findings are noteworthy in the consideration of catalyst developments for chemoselective functionalization.

DFT based calculations

We have investigated the reaction mechanism of **Mn-3** catalyzed hydrogenation of α,β-unsaturated carbonyl compound **4a** using density functional theory (DFT) calculations (Fig. 3). Initially, the generation of the active catalyst **A** would occur when the pre-catalyst **Mn-3** reacts with K_3PO_4 (Fig. 3(I)). In this step, the Mn–Br and N–H bonds break, forming the catalyst **A**, K_2HPO_4 and KBr. This step is thermodynamically favorable ($\Delta G = -19.9$ kcal mol^{-1}). Next, the H_2 molecule adds to catalyst **A**, forming the intermediate **B** *via* a barrier of 14.7 kcal mol^{-1} (**TS-1**). Then, the reaction proceeds through **TS-2** with a barrier of 21.7 kcal mol^{-1}, in which the H–H bond breaks, and the Mn–H and N–H bonds form, generating the intermediate **C**. The overall barrier for the H_2 activation (31.3 kcal mol^{-1}) seems reasonable, considering that a minimum of 5 bar H_2 pressure is essential for the reaction. In the next step, the reaction crosses the barrier of 9.1 kcal mol^{-1} (**TS-3**), wherein **4a** reacts with **C** to form the intermediate **D** by hydride (H^-) migration from Mn–H to **4a**. In the next step, the intermediate **D** rearranges and forms a new intermediate **E**. This step is found to be thermodynamically favorable ($\Delta G = -5.2$ kcal mol^{-1}).

Starting with the intermediate **E**, two approaches are considered for protonation (Fig. 3(II)). In the first possibility, the methanol protonates the substrate step-wise, as shown in Fig. 3(II). Thus, MeOH can provide a proton to the substrate and coordinates with Mn concurrently. In this process, the Mn–O bond breaks and a different Mn–O bond forms *via* the transition state **TS-4** with a barrier of 10.7 kcal mol^{-1}, leading to the formation of the intermediate **F**. The reaction crosses a barrier of 1.1 kcal mol^{-1} (**TS-5**) in the following step, leading to product **4** and intermediate **G**. Then, the reaction could proceed in two different ways: with the assistance of solvent (MeOH) **TS-6** and without the assistance of solvent **TS-6′**, which has barriers of 6.8 kcal mol^{-1} and 14.6 kcal mol^{-1}, respectively. The energy values indicate that the reaction will proceed through the transition state **TS-6** with the assistance of a solvent (MeOH), leading to the formation of intermediate **H**. In the next step, intermediate **H** is converted into **A** after releasing methanol. This step is thermodynamically favorable ($\Delta G = -4.4$ kcal mol^{-1}). The overall low barrier for the protonation process tentatively supports the experimental observation, wherein a reversible protonation was assumed.

In the second possibility of protonation, the solvent MeOH directly shuttles the protons between Mn–O and N–H through a transition state **TS-7** with a barrier of 11.0 kcal mol^{-1}, leading to the formation of intermediate **I** (Fig. 3(II)). In the next step, intermediate **I** is converted into the active species **A** and product **4**. This step is thermodynamically favorable ($\Delta G = -18.5$ kcal mol^{-1}). A perusal of the two pathways based on turnover frequency (TOF) analysis indicates that the TOF would be the same for both approaches (Fig. 3(II)), because the main intermediate (TDI) (**A**) along the pathways and the main transition state (TDTS) (**TS-2**) are present in the early part of the cycles, which are common to both the proposed protonation pathways (for more information on the TOF analysis, see the ESI†). The calculated energy barrier values indicated a maximum barrier for H_2 activation, which would be feasible at room temperature considering the reaction's 5.0 bar H_2

© 2022 The Author(s). Published by the Royal Society of Chemistry

Open Access Article. Published on 03 2022. Downloaded on 01.02.2026 18:25:54.
This article is licensed under a Creative Commons Attribution-NonCommercial 3.0 Unported Licence.

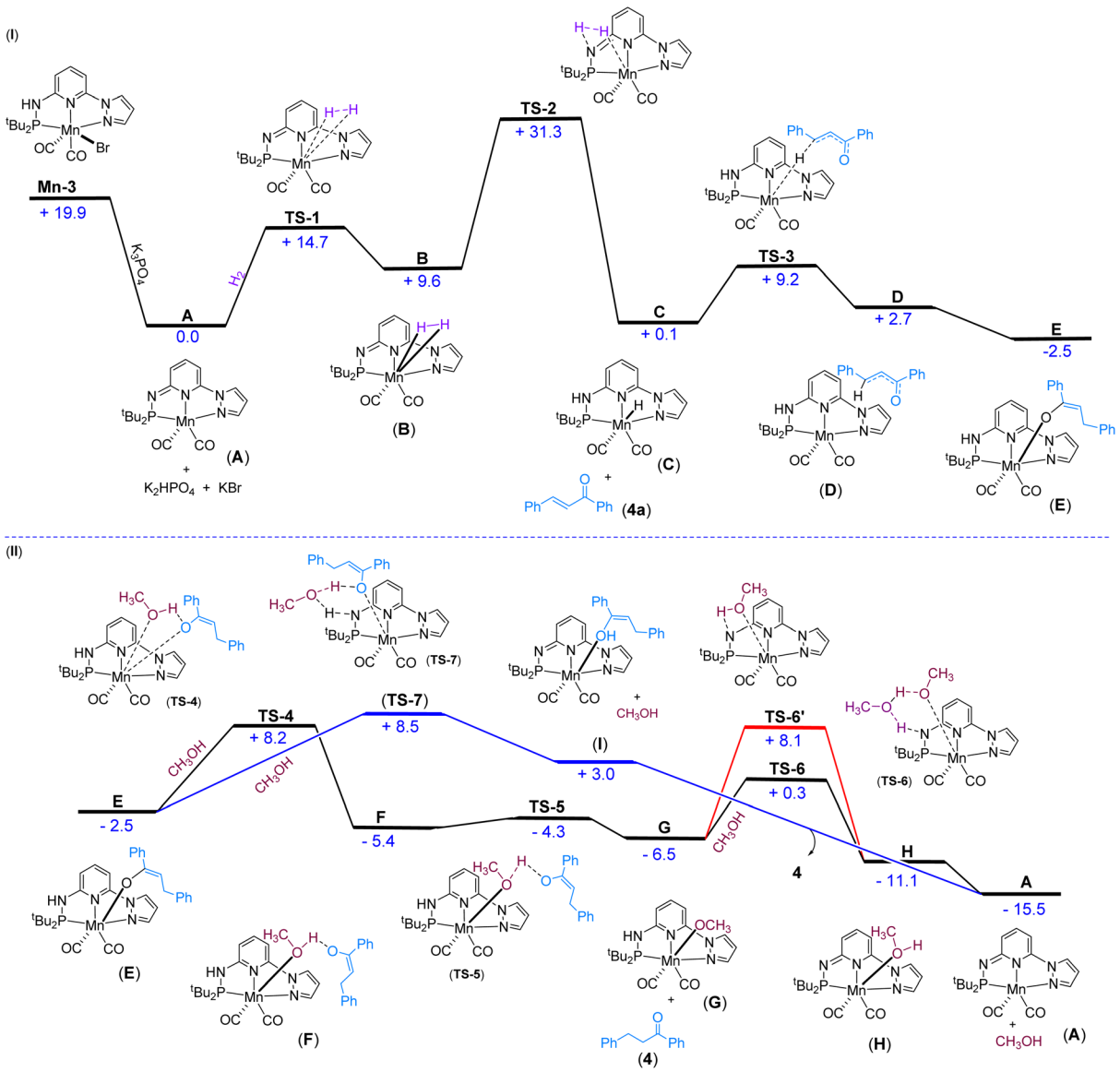

Fig. 3 Free energy profile for (^{tBu}PNN^{Pyz}) Mn(I)-catalyzed hydrogenation: (I) **Mn-3** to intermediate **E**, (II) intermediate **E** to regeneration of active catalyst **A**. The free energy values are given in kcal mol^{-1}.

pressure requirement. Therefore, H_2 activation could be proposed as a probable turnover-limiting step. Notably, the protonation of the final compound by MeOH is very facile, which corroborates the experimental findings.

Catalytic cycle

Based on the experimental findings, DFT calculations and literature precedents,[12a,15c,21b] we proposed a tentative catalytic cycle for the Mn-catalyzed chemoselective hydrogenation of α,β-unsaturated ketones (Fig. 4). Initially, the complex **Mn-3** would transform into the active catalyst **A** by dearomatization in the presence of K_3PO_4. We have identified the species **A** by NMR and IR analyses. The similar conversion of a metal complex into dearomatized species is well documented.[12a,21b,24] Moreover, the species **A** as an active catalyst was verified. The H_2 molecule will coordinate to Mn(I) species, followed by metal–ligand (M–L) cooperative activation of H_2 leading to species **C** through transition state **TS-2**. Next, the reaction of substrate **4a** with **C** leads to 1,4-hydride migration resulting in intermediate **D** (or **E**). The protonation of the semi-hydrogenated species in intermediate **D** (or **E**) by methanol provides the hydrogenated product **4**. Finally, the resulting intermediate **G** would lead to the regeneration of active catalyst **A**. The DFT energy calculations supported all these elementary catalytic steps. H_2 activation by the Mn(I) species has a high barrier and is a pivotal step in the hydrogenation process. Therefore, H_2 activation by Mn(I)–ligand cooperation can be assumed to be the turnover-limiting step.

© 2022 The Author(s). Published by the Royal Society of Chemistry

Open Access Article. Published on 03 2022. Downloaded on 01.02.2026 18:25:54.
This article is licensed under a Creative Commons Attribution-NonCommercial 3.0 Unported Licence.

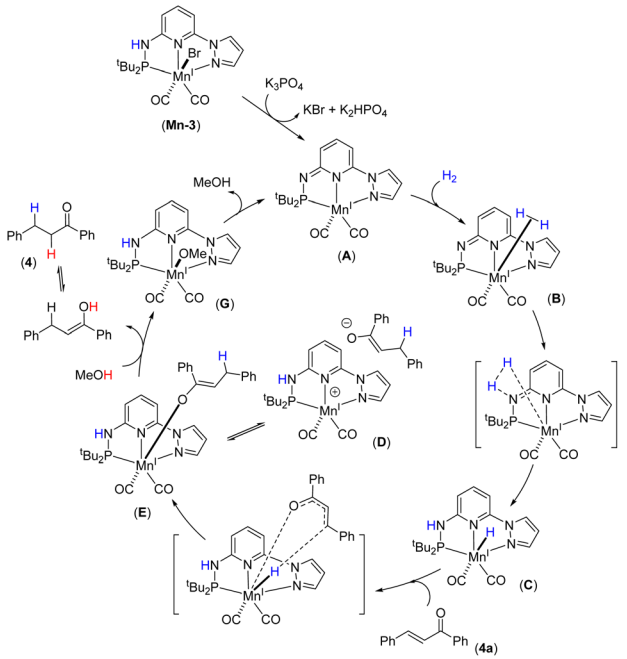

Fig. 4 Plausible catalytic cycle.

Conclusions

In summary, we have developed an efficient protocol for the chemoselective hydrogenation of C=C, C=O and C=N bonds in α,β-unsaturated ketones, aldehydes and imines catalyzed by the well-defined pincer-ligated Mn(I) complex. The employment of a mild base, moderate H_2 pressure and room temperature (27 °C) in Mn-catalyzed hydrogenation are highly advantageous to the commonly employed KO^{t}Bu base and extreme reaction conditions. The mixed donor Mn(I) complexes, κ^3-(^{R2}PN^{3}N^{Pyz})Mn(CO)$_2$Br (R = Ph, ^{i}Pr, ^{t}Bu) were synthesized and meticulously characterized by various techniques. Though both the ^{i}Pr and ^{t}Bu-substituted Mn(I) complexes are efficient for the hydrogenation of α,β-unsaturated ketones, the (^{tBu2}PNN^{Pyz})Mn(CO)$_2$Br complex as a catalyst provided exceptional chemoselectivity for the reduction of the C=C bond (1,4-hydrogen addition). Thus, using the beneficial molecular hydrogen and a mild K_3PO_4 base, the (^{tBu2}PNN^{Pyz})Mn(I) catalyst could hydrogenate diverse unsaturated ketones to saturated ketones at room temperature with the compatibility of sensitive functionalities, such as halides (–F, –Cl, –Br, and –I), alkoxy, hydroxy, epoxide, acetyl, nitrile, nitro, and unconjugated alkenyl and alkynyl groups. The C=O bond in aldehydes and the C=N bond in imines were preferentially hydrogenated (1,2-hydrogen addition) over the C=C bond using the **Mn-3** catalyst. A comprehensive mechanistic investigation by controlled studies endorsed the non-innocent behavior of the ligand in the Mn catalyst and supported a metal–ligand cooperation pathway. The DFT energy calculations highlighted a probable turnover-limiting H_2 activation with the facile progress of other elementary steps. Particularly, H_2 provided a hydride source, and solvent MeOH acts as a proton source for hydrogenation. The DFT energy calculations unanimously supported the proposed mechanistic cycle.

Data availability

Crystallographic data for compound **Mn-2** has been deposited at The Cambridge Crystallographic Data Centre (CCDC) under deposition number 2194541.†

Author contributions

A. B. S. and D. M. S. designed and performed the catalyst synthesis. A. B. S. carried out all catalytic and mechanistic experiments. A. B. S. and B. P. conceived the project, interpreted the results and co-wrote the original draft. R. G. G. performed XRD and analysed the data. P. B. performed DFT calculations under the supervision of K. V. All authors contributed to the analysis of the results and preparation of the manuscript.

Conflicts of interest

There are no conflicts to declare.

Acknowledgements

This work was financially supported by SERB, New Delhi, India (CRG/2020/000554). A. B. S. and D. M. S. thank CSIR-New Delhi for research fellowships. We acknowledge the National Supercomputing Mission (NSM) for providing computing resources of 'PARAM Brahma' at IISER Pune, which is implemented by C-DAC and supported by the Ministry of Electronics and Information Technology (MeitY) and Department of Science and Technology (DST), Government of India.

Notes and references

1 (*a*) P. N. Rylander, Catalytic Hydrogenation in Organic Synthesis, in *The Catalytic Hydrogenation in Organic Syntheses*, Academic Press, New York, 1979, pp. 1–12; (*b*) P. G. Andersson and I. J. Munslow, *Modern Reduction Methods*, Wiley-VCH Verlag GmbH & Co., 2008.

2 (*a*) J. Pritchard, G. A. Filonenko, R. van Putten, E. J. M. Hensen and E. A. Pidko, *Chem. Soc. Rev.*, 2015, **44**, 3808–3833; (*b*) M. Tamura, Y. Nakagawa and K. Tomishige, *J. Jpn. Petroleum Inst.*, 2019, **62**, 106–119; (*c*) Y. Wang, M. Wang, Y. Li and Q. Liu, *Chem*, 2021, **7**, 1180–1223.

3 J. G. de Vries and C. J. Elsevier, *Handbook of Homogeneous Hydrogenation*, Weinheim Wiley-VCH, 2007.

4 (*a*) R. Noyori and T. Ohkuma, *Angew. Chem., Int. Ed.*, 2001, **40**, 40–73; (*b*) J.-H. Xie, S.-F. Zhu and Q.-L. Zhou, *Chem. Rev.*, 2011, **111**, 1713–1760; (*c*) M. L. Clarke, *Catal. Sci. Technol.*, 2012, **2**, 2418–2423; (*d*) D.-S. Wang, Q.-A. Chen, S.-M. Lu and Y.-G. Zhou, *Chem. Rev.*, 2012, **112**, 2557–2590; (*e*) S. Werkmeister, K. Junge and M. Beller, *Org. Pro. Res. Dev.*, 2014, **18**, 289–302; (*f*) Y.-M. He, Y. Feng and Q.-H. Fan, *Acc. Chem. Res.*, 2014, **47**, 2894–2906.

© 2022 The Author(s). Published by the Royal Society of Chemistry

Open Access Article. Published on 03 2022. Downloaded on 01.02.2026 18:25:54.
This article is licensed under a Creative Commons Attribution-NonCommercial 3.0 Unported Licence.

5 (*a*) G. A. Filonenko, R. van Putten, E. J. M. Hensen and E. A. Pidko, *Chem. Soc. Rev.*, 2018, **47**, 1459–1483; (*b*) T. Zell and R. Langer, *ChemCatChem*, 2018, **10**, 1930–1940; (*c*) L. Alig, M. Fritz and S. Schneider, *Chem. Rev.*, 2019, **119**, 2681–2751; (*d*) T. Irrgang and R. Kempe, *Chem. Rev.*, 2019, **119**, 2524–2549.

6 (*a*) I. Bauer and H.-J. Knölker, *Chem. Rev.*, 2015, **115**, 3170–3387; (*b*) T. Zell and D. Milstein, *Acc. Chem. Res.*, 2015, **48**, 1979–1994; (*c*) S. Chakraborty, P. Bhattacharya, H. Dai and H. Guan, *Acc. Chem. Res.*, 2015, **48**, 1995–2003; (*d*) A. Fürstner, *ACS Cent. Sci.*, 2016, **2**, 778–789.

7 (*a*) A. Mukherjee and D. Milstein, *ACS Catal.*, 2018, **8**, 11435–11469; (*b*) W. Liu, B. Sahoo, K. Junge and M. Beller, *Acc. Chem. Res.*, 2018, **51**, 1858–1869; (*c*) W. Ai, R. Zhong, X. Liu and Q. Liu, *Chem. Rev.*, 2019, **119**, 2876–2953.

8 (*a*) R. M. Bullock, *Science*, 2013, **342**, 1054–1055; (*b*) W. Zuo, A. J. Lough, Y. F. Li and R. H. Morris, *Science*, 2013, **342**, 1080–1083; (*c*) M. R. Friedfeld, M. Shevlin, J. M. Hoyt, S. W. Krska, M. T. Tudge and P. J. Chirik, *Science*, 2013, **342**, 1076–1080; (*d*) M. R. Friedfeld, H. Zhong, R. T. Ruck, M. Shevlin and P. J. Chirik, *Science*, 2018, **360**, 888–893.

9 S. Elangovan, C. Topf, S. Fischer, H. Jiao, A. Spannenberg, W. Baumann, R. Ludwig, K. Junge and M. Beller, *J. Am. Chem. Soc.*, 2016, **138**, 8809–8814.

10 F. Kallmeier, T. Irrgang, T. Dietel and R. Kempe, *Angew. Chem., Int. Ed.*, 2016, **55**, 11806–11809.

11 (*a*) A. Bruneau-Voisine, D. Wang, T. Roisnel, C. Darcel and J.-B. Sortais, *Catal. Commun.*, 2017, **92**, 1–4; (*b*) D. Wei, A. Bruneau-Voisine, T. o. Chauvin, V. Dorcet, T. Roisnel, D. A. Valyaev, N. l. Lugan and J.-B. Sortais, *Adv. Synth. Catal.*, 2018, **360**, 676–681; (*c*) R. Buhaibeh, O. A. Filippov, A. Bruneau-Voisine, J. Willot, C. Duhayon, D. A. Valyaev, N. Lugan, Y. Canac and J.-B. Sortais, *Angew. Chem., Int. Ed.*, 2019, **58**, 6727–6731; (*d*) R. Buhaibeh, C. Duhayon, D. A. Valyaev, J.-B. Sortais and Y. Canac, *Organometallics*, 2021, **40**, 231–241.

12 (*a*) M. Glatz, B. Stöger, D. Himmelbauer, L. F. Veiros and K. Kirchner, *ACS Catal.*, 2018, **8**, 4009–4016; (*b*) S. Weber, B. Stöger and K. Kirchner, *Org. Lett.*, 2018, **20**, 7212–7215; (*c*) S. Weber, J. Brünig, L. F. Veiros and K. Kirchner, *Organometallics*, 2021, **40**, 1388–1394.

13 (*a*) H.-J. Pan and X. Hu, *Angew. Chem., Int. Ed.*, 2020, **59**, 4942–4946; (*b*) W. Yang, I. Y. Chernyshov, R. K. A. van Schendel, M. Weber, C. Müller, G. A. Filonenko and E. A. Pidko, *Nat. Commun.*, 2021, **12**, 12; (*c*) T. Vielhaber and C. Topf, *Appl. Catal. A: Gen.*, 2021, **623**, 118280.

14 For reviews, see: (*a*) B. Maji and M. K. Barman, *Synthesis*, 2017, **49**, 3377–3393; (*b*) M. Garbe, K. Junge and M. Beller, *Eur. J. Org. Chem.*, 2017, **2017**, 4344–4362; (*c*) F. Kallmeier and R. Kempe, *Angew. Chem., Int. Ed.*, 2018, **57**, 46–60; (*d*) N. Gorgas and K. Kirchner, *Acc. Chem. Res.*, 2018, **51**, 1558–1569.

15 (*a*) D. Wei, A. Bruneau-Voisine, D. A. Valyaev, N. Lugan and J.-B. Sortais, *Chem. Commun.*, 2018, **54**, 4302–4305; (*b*) Y. Wang, L. Zhu, Z. Shao, G. Li, Y. Lan and Q. Liu, *J. Am. Chem. Soc.*, 2019, **141**, 17337–17349; (*c*) F. Freitag, T. Irrgang and R. Kempe, *J. Am. Chem. Soc.*, 2019, **141**, 11677–11685; (*d*) Z. Wang, L. Chen, G. Mao and C. Wang, *Chin. Chem. Lett.*, 2020, **31**, 1890–1894; (*e*) Y. Wang, S. Liu, H. Yang, H. Li, Y. Lan and Q. Liu, *Nat. Chem.*, 2022, **14**, 1233–1241.

16 M. B. Widegren, G. J. Harkness, A. M. Z. Slawin, D. B. Cordes and M. L. Clarke, *Angew. Chem., Int. Ed.*, 2017, **56**, 5825–5828.

17 (*a*) M. Garbe, K. Junge, S. Walker, Z. Wei, H. Jiao, A. Spannenberg, S. Bachmann, M. Scalone and M. Beller, *Angew. Chem., Int. Ed.*, 2017, **56**, 11237–11241; (*b*) M. Garbe, Z. Wei, B. Tannert, A. Spannenberg, H. Jiao, S. Bachmann, M. Scalone, K. Junge and M. Beller, *Adv. Synth. Catal.*, 2019, **361**, 1913–1920.

18 (*a*) L. Zhang, Y. Tang, Z. Han and K. Ding, *Angew. Chem., Int. Ed.*, 2019, **58**, 4973–4977; (*b*) L. Zhang, Z. Wang, Z. Han and K. Ding, *Angew. Chem., Int. Ed.*, 2020, **59**, 15565–15569.

19 (*a*) F. Ling, H. Hou, J. Chen, S. Nian, X. Yi, Z. Wang, D. Song and W. Zhong, *Org. Lett.*, 2019, **21**, 3937–3941; (*b*) L. Zeng, H. Yang, M. Zhao, J. Wen, J. H. R. Tucker and X. Zhang, *ACS Catal.*, 2020, **10**, 13794–13799; (*c*) F. Ling, J. Chen, S. Nian, H. Hou, X. Yi, F. Wu, M. Xu and W. Zhong, *Synlett*, 2020, **31**, 285–289; (*d*) C. S. G. Seo, B. T. H. Tsui, M. V. Gradiski, S. A. M. Smith and R. H. Morris, *Catal. Sci. Technol.*, 2021, **11**, 3153–3163.

20 (*a*) C. Liu, M. Wang, S. Liu, Y. Wang, Y. Peng, Y. Lan and Q. Liu, *Angew. Chem., Int. Ed.*, 2021, **60**, 5108–5113; (*b*) C. Liu, M. Wang, Y. Xu, Y. Li and Q. Liu, *Angew. Chem., Int. Ed.*, 2022, **61**, DOI: **10.1002/anie.202202814**.

21 (*a*) S. Weber, B. Stöger, L. F. Veiros and K. Kirchner, *ACS Catal.*, 2019, **9**, 9715–9720; (*b*) S. M. W. Rahaman, D. K. Pandey, O. Rivada-Wheelaghan, A. Dubey, R. R. Fayzullin and J. R. Khusnutdinova, *ChemCatChem*, 2020, **12**, 5912–5918.

22 For selected chemoselective hydrogenation using **4d** metals, see: (*a*) Q. Hu, Y. Hu, Y. Liu, Z. Zhang, Y. Liu and W. Zhang, *Chem.–Eur. J.*, 2017, **23**, 1040–1043; (*b*) W. Chang, X. Gong, S. Wang, L.-P. Xiao and G. Song, *Org. Biomol. Chem.*, 2017, **15**, 3466–3471; (*c*) M. Soto, R. G. Soengas and H. Rodríguez-Solla, *Adv. Synth. Catal.*, 2020, **362**, 5422–5431; (*d*) Y. Gu, J. R. Norton, F. Salahi, V. G. Lisnyak, Z. Zhou and S. A. Snyder, *J. Am. Chem. Soc.*, 2021, **143**, 9657–9663.

23 (*a*) D. Gong, W. Liu, T. Chen, Z.-R. Chen and K.-W. Huang, *J. Mol. Catal. A Chem.*, 2014, **395**, 100–107; (*b*) D. Gong, X. Zhang and K.-W. Huang, *Dalton Trans.*, 2016, **45**, 19399–19407; (*c*) H. Chen, W. Pan, K.-W. Huang, X. Zhang and D. Gong, *Polym. Chem.*, 2017, **8**, 1805–1814.

24 (*a*) T. P. Gonçalves and K.-W. Huang, *J. Am. Chem. Soc.*, 2017, **139**, 13442–13449; (*b*) T. Shimbayashi and K.-i. Fujita, *Catalysts*, 2020, **10**, 635.

© 2022 The Author(s). Published by the Royal Society of Chemistry